Title

Minimizing echo and repetition times in magnetic resonance imaging using a double half-echo k-space acquisition and low-rank reconstruction

Journal

NMR in Biomedicine, 34(4)

ISSN

0952-3480

Authors

Bydder, Mark
Ali, Fadil
Ghodrati, Vahid
et al.

Publication Date

2021-04-01

DOI

10.1002/nbm.4458

Peer reviewed

HHS Public Access

Author manuscript

NMR Biomed. Author manuscript; available in PMC 2022 April 01.

Published in final edited form as:

NMR Biomed. 2021 April ; 34(4): e4458. doi:10.1002/nbm.4458.

Minimizing Echo and Repetition Times in Magnetic Resonance Imaging Using a Double Half-Echo *k*-Space Acquisition And Low-Rank Reconstruction

Mark Bydder[1,*], **Fadil Ali**[1], **Vahid Ghodrati**[1], **Peng Hu**[1], **Jingwen Yao**[1,2], **Benjamin M. Ellingson**[1,2,3]

[1]Department of Radiological Sciences, David Geffen School of Medicine, University of California Los Angeles, Los Angeles, CA

[2]Department of Bioengineering, Samueli School of Engineering, University of California Los Angeles, Los Angeles, CA

[3]Department of Psychiatry and Biobehavioral Sciences, David Geffen School of Medicine, University of California Los Angeles, Los Angeles, CA

Abstract

Sampling *k*-space asymmetrically (i.e. “partial Fourier sampling”) in the readout direction is a common way to reduce the echo time (TE) during magnetic resonance image acquisitions. This technique requires overlap around the center of *k*-space to provide a calibration region for reconstruction, which limits the minimum fractional echo to ~60% before artifacts are observed. The present study describes a method for reconstructing images from exact half echoes using two separate acquisitions with reversed readout polarity, effectively providing a full line of *k*-space without additional data around central *k*-space. This approach can benefit sequences or applications that prioritize short TE, short inter-echo spacing or short repetition time (TR). An example of the latter is demonstrated to reduce banding artifacts in balanced steady state free procession.

INTRODUCTION

In magnetic resonance imaging (MRI), fractional sampling along the readout direction is a well-known strategy for reducing the echo time (TE)[1]. This is useful for capturing signals from short T2 species but also reduces the inter-echo spacing (ΔTE) and repetition time (TR). Reconstruction by simple Fourier transform is not possible from fractionally sampled datasets, so various algorithms have been developed to produce relatively artifact-free images based on an assumption that there is smooth phase across the image.

[*]**Corresponding author:** Mark Bydder, Ph.D., Department of Radiological Sciences, David Geffen School of Medicine, University of California, Los Angeles, 924 Westwood Blvd., Suite 615, Los Angeles, CA 90024, Phone: 310-268-6842, Fax: 310-794-2796.

Conflicts of Interest:

BME is an advisor for Hoffman La-Roche; Siemens; Nativis; Medicenna; MedQIA; Bristol Meyers Squibb; Imaging Endpoints; VBL; and Agios Pharmaceuticals. BME is a Paid Consultant for Nativis; MedQIA; Siemens; Hoffman La-Roche; Imaging Endpoints; Medicenna; and Agios. BME received grant funding from Siemens, Agios, and Janssen.

The typical minimum echo fraction is around 60% and artefacts are usually apparent by this point. Further reduction of the echo fraction could allow for more of the T2-decaying signal to be acquired (Table 1) but reconstruction algorithms become less effective because the area of overlap about the point of conjugate symmetry is reduced. Examples of image reconstruction using different echo fractions are shown in Figure 1 using a contemporary method that represents conjugate reflection as a low-rank problem[2]. Note that the image quality decreases with echo fraction and is unusable at 50%.

One way to approach the 50% limit is to acquire two readouts with the gradient polarity in opposite directions, as depicted in Figure 2. While the individual half echoes themselves cannot be reconstructed, the paired acquisition can be combined to obtain complete *k*-space sampling along the readout direction. This effectively provides a full echo of *k*-space data with the TE of a half-echo acquisition but at a cost of increasing the acquisition time. Similar half echo acquisition schemes have been developed for ultrashort TE imaging and flow artefact suppression[3–4].

The simplest reconstruction of the paired acquisition is to directly insert data into the *k*-space matrix where it nominally belongs (referred to as the “drop in place” algorithm) followed by Fourier transform. A challenge is that the center of *k*-space is acquired at the end of a gradient ramp; as discussed in Young *et al*[5], short term eddy currents can act as a low-pass filter that modify the ramp and alter the *k*-space trajectory (Figure 3). With fully sampled readouts this occurs at the edge of *k*-space and is benign in terms of any resulting image artifacts.

Deviation from Cartesian sampling at the earliest time-point and the transient effects of switching on the ADC (analog-to-digital conversion) are difficult to model and are best avoided by discarding the first microseconds of data[3]. Once the gradient amplitude has stabilized there remains a constant offset (aka gradient delay) between the ideal and actual *k*-space coordinates. Calibration for the gradient delay is required whenever readout gradient directions are varied within a sequence (e.g. radial, bipolar, forward/reverse schemes)[6–8]. Since the delays depend on the physical axis, gradient amplitude and distance from isocenter, the correction can be somewhat involved[5].

The situation depicted in Figure 2 can be viewed as the reverse of an approach used for echo planar imaging (EPI) ghost correction[9–10], where a single dataset containing forward (left-to-right) and reverse (right-to-left) lines of *k*-space are split into two undersampled datasets consisting of pure forward and pure reverse lines. Reconstruction of the undersampled datasets is performed simultaneously with a coupling constraint that enforces similarity up to a convolution in *k*-space with a small shift-invariant kernel. The kernels represent differences between the datasets that can be represented as convolution in *k*-space, which include the effects of gradient delays (phase roll across the field-of-view), coil shading (parallel imaging) and conjugate symmetry (partial Fourier)[2,11]. The reconstructed images from the forward/reverse lines are free of ghosting caused by the gradient delay and may be combined into a single image[9].

The goal of the present study is to explore the feasibility of a double half-echo acquisition using low-rank reconstruction to minimize the TE, ΔTE and TR beyond those currently used in Cartesian MRI.

METHODS

All data were acquired on a 3T system (Siemens Prisma Fit, Erlangen, Germany) using a 2-channel transmit/receive body coil. A 2D gradient echo sequence was used with spoiled gradient recalled echo (SPGR) or balanced steady state free procession (bSSFP) readouts and an asymmetric 0.6 ms RF pulse, as represented in Figure 4. The sequence preparation used the highest gradient performance settings and the shortest possible durations.

Reconstructions were performed offline in Matlab 2020a (Natick, MA) on a Nvidia RTX4000 GPU (Santa Clara, CA) and took 10 seconds for simple double half echo combination and up to 10 minutes for partial/parallel accelerated datasets. Care was taken to prevent the raw data handling software from improperly removing readout oversampling.

The algorithm used for low rank reconstruction is based on matrix completion incorporating coils, conjugate symmetry and half echoes stacked along the rows as illustrated in Figure 5 and summarized in Table 2.[11–12] A MATLAB implementation *dhe.m* is available online at https://github.com/marcsous/parallel. The process of rank reduction identifies correlations along the rows, which should only differ by coil shading and/or low-resolution phase variations. An important step in the algorithm is to suppress small singular values in the data matrix. Letting s_k be the k^{th} singular value and σ_{floor} be the noise floor of the singular values (see Appendix), singular value shrinkage is effected using the filter $0 \leq f_k \leq 1$ as follows:

$$s_k = f_k \cdot s_k \,[\text{shrinkage}]$$

$$f_k = \max\left(1 - \sigma_{floor}/s_k,\ 0\right) [\text{soft threshold}]$$

$$f_k = \max\left(1 - \sigma_{floor}^2/s_k^2,\ 0\right) [\text{minimum variance}]$$

These filter choices are associated with the nuclear and Frobenius norms, respectively[13–14] and the iterative reconstruction compresses the energy of the singular values in a way that corresponds with the norm of the data matrix. Initial results suggested that the minimum variance filter gave more similar results to the unaliasing performance and *g*-factor noise of conventional MRI algorithms; the design of singular value filters for different cases is an active research topic[15].

RESULTS

Application of Double Half-Echo Acquisition to bSSFP

While short TE is not necessarily a priority with bSSFP, reducing the readout duration also reduces the minimum attainable TR and decreases susceptibility artefacts. The decrease in TR absorbs some of the time cost of using two acquisitions. Figure 6 shows images reconstructed from a full *k*-space readout and examples of double half echoes (using two opposed readouts) using 66% and 50% partial echoes. The off-resonance banding artifacts are reduced in inverse proportion to the TR.

Robustness to Gradient Delays

To test the robustness to gradient delays an acquisition was made with small delays applied to the readout gradient. Results in Figure 7 compare a simple “drop in place” algorithm (top row) versus the low rank algorithm (bottom row). Delay parameters must be tuned carefully with the former approach and the best choice (somewhere between 0 and 1 μs) still leaves residual artefacts. In contrast, the latter approach is completely robust to delays of more than 2 dwell times.

Combination with Partial/Parallel Imaging Methods

Low rank reconstruction is well-suited to parallel imaging and partial Fourier reconstruction[2,11], since they conform to the requirement of similarity up to a small shift-invariant convolution. Therefore partial/parallel acquisitions are expected to be compatible with double half echoes. Figure 8 confirms the compatibility using an example of 5/8 partial plus 2-fold parallel acceleration in the phase encode direction and double half echoes in the readout direction. The reconstruction was repeated twice using different singular value filters, indicating convergence to different solutions. Difference in noise and residual aliasing are similar to the effects of regularization in least-squares reconstruction algorithms.

Combination of the Final Images

The double half-echo reconstruction produces one complex image per coil per gradient direction. The coils can be adaptively combined to maximize the signal-to-noise ratio (SNR), which leaves two images (fwd and rev). These may be combined by sum of squares[9] although the noise is highly correlated due to the reconstruction method used so an assumption of independent and identical distribution is not met. Table 3 confirms that the fwd, rev and combined images do not show any SNR benefit from combination. Furthermore, differences between fwd and rev capture physical effects in the images, such as B_0 field inhomogeneities, gradient delays; correcting for these effects would allow for further refinement of the reconstruction but is beyond the scope of the present study.

DISCUSSION

The present article has described a method to recover artifact free images from half echo datasets, which provides access to shorter TE, ΔTE and TR in Cartesian acquisitions. The method is based on low-rank reconstruction, similar to SAKE and LORAKS, and is fully compatible with these acceleration techniques[2,11]. Low-rank reconstruction methods extend

easily to include changes in the sampling pattern and temporal dimensions (including echoes), if suitable data is available[16–17]. These forms of redundancy have been used previously in image reconstruction[18–21] but are particularly straightforward when used with low-rank methods.

An example of fractional echo bSSFP was described previously for ultra-fast bSSFP (ufSFFP) imaging of the lung using an overlap of 13 % about the center of *k*-space[22]. Reducing the overlap to 0 % using the technique outlined in the present study could further decrease the TR and improve robustness to susceptibility and/or permit an increase in spatial resolution. The RF excitation can also be shortened to a half pulse to reduce the TR but would require two additional acquisitions with alternating slice select gradients[4].

The shorter available TE and ΔTE may be useful in applications such as short T2 non-proton imaging and multi-echo water-fat separation. An example of a multi-echo readout is given in Figure 4; the ΔTE between echoes 2 and 3 can be as short as two ramp times (on the order of 100 μs) to mitigate ΔB_0 frequency aliasing or may be increased to provide equal spacing. Alternative segmented readout schemes are possible.[23] Other applications that blend data with different spin histories may also be compatible with low rank reconstruction. Hexagonal spoiling utilizes 4 or 6 different gradient directions from TR to TR that may prevent cancellation of long-term eddy currents.[24] Segmenting the data into bins according to the spoiler direction would allow differences to be modeled out and removed.

The current study has several limitations. First, image reconstruction is slow for clinical use. The algorithm implemented in the present study (based on Ref 11) is inefficient compared to recent implementations[25] however it is robust and has minimal tuning parameters: only the noise variance and kernel size are needed. Prior research has shown low rank reconstructions provide robust image quality on *in vivo* data, however in a clinical setting it may be necessary to demonstrate clear advantages over conventional approaches to justify the higher computational overhead.

Second, chemical shift artifacts can manifest in all the readout directions used. These are not modeled by shift invariant convolutions and therefore will remain in the images, potentially causing misleading artifacts at low bandwidth (c.f. center-out radial[26]).

Lastly, the low rank method yields images for both forward and reverse data sets. Sum of squares combination is not effective since the image noise is correlated, and moreover the images contain physical differences that potentially can be used to correct artefacts due to chemical shift or spatial distortion[27].

CONCLUSION

The present study has described a method for reconstructing images from half echoes acquired in separate acquisitions using reversed readout polarity to provide a full line of *k*-space. The approach is beneficial in applications that prioritize short TE, short ΔTE or TR.

ACKNOWLEDGEMENTS

The authors thank Prof. Dieter Enzmann (UCLA, Los Angeles) for his continued support and Prof. Peter Gatehouse (Royal Brompton Hospital, London) for helpful discussions.

Funding: UCLA Radiology Sodium MRI Research Program; American Cancer Society (RSG-15-003-01-CCE) (Ellingson); NIH/NCI 1P50CA211015-01A1 (Ellingson); NIH/NCI 1R21CA223757-01 (Ellingson); NIH/NINDS 2R01NS078494-06 (Ellingson); NIH/NIDDK U54 DK064539 (Ellingson)

Appendix: estimation of the noise floor

The "Additive noise and missing at random" contamination model of Ref 15 defines $m \times n$ matrix **A** as the sum of a low rank matrix **X** plus a noise matrix **Z** whose elements are drawn from a Gaussian distribution with standard deviation σ. Entries are missing (zero) with probability $1 - \kappa$. Assuming $m \gg n$, **X** may be approximated from **A** by modifying the singular values (s) to:

$$\eta \approx \left[1 - \frac{\sigma^2 m\kappa}{s^2}\right] \cdot s$$

This is comparable with the minimum variance filter for $\sigma_{floor} = \sigma \cdot \sqrt{m\kappa}$, which is a measure of central tendency of the singular values of **Z**. In estimating σ_{floor}, two practical cases arise: (i) σ is known (e.g. from prescan measurements), in which case σ_{floor} is easily calculated from the data size m and sampling κ; or (ii) σ is not known, in which case, a heuristic based on the median value of s can be used.[15] Other schemes may be devised using the fact that small singular values mainly reflect the noise.

Abbreviations Used:

ADC	analog-to-digital conversion
TE	echo time
TR	repetition time
bSSFP	balanced steady state free procession
ufSSFP	ultra fast balanced steady state free procession
MRI	magnetic resonance imaging
EPI	echo planar imaging
SAKE	simultaneous autocalibrating and *k*-space estimation
LORAKS	low-rank modeling of local *k*-space neighborhoods
SNR	signal to noise ratio
ROI	region of interest

REFERENCES

1. Bernstein MA, King KF, Zhou XJ. Handbook of MRI Pulse Sequences: Elsevier Academic Press; 2004. Chapter 13.4
2. Haldar JP. Low-rank modeling of local k-space neighborhoods (LORAKS) for constrained MRI. IEEE Trans Med Imaging. 2014; 33(3):668–681. [PubMed: 24595341]
3. Scheidegger MB, Maier SE, Boesiger P. FID-Acquired-Echos: A short echo time imaging method for flow artefact suppression. Magnetic Resonance Imaging 1991; 9(4): 517–524 [PubMed: 1779722]
4. Robson MD, Gatehouse PD, Bydder M, Bydder GM. Magnetic resonance: an introduction to ultrashort TE imaging. J Comput Assist Tomogr. 2003;27(6):825–846 [PubMed: 14600447]
5. Young IR, Bydder GM, Fullerton GD. MRI of Tissues with Short T2s or T2*s: John Wiley & Sons; 2012. Chapter 7
6. Tan H, Meyer CH. Estimation of k-space trajectories in spiral MRI. Magn Reson Med. 2009; 61(6):1396–1404. [PubMed: 19353671]
7. Bydder M, Yokoo T, Du J. Automatic calculations of gradient delays for center-out radial trajectories using en entropy metric. Paper presented at: Proc Int Soc Magn Reson Med 2007.
8. Jiang W, Larson PEZ, Lustig M. Simultaneous auto-calibration and gradient delays estimation in non-Cartesian parallel MRI using low-rank constraints. Magn Reson Med. 2018; 80(5):2006–2016. [PubMed: 29524244]
9. Lee J, Jin KH, Ye JC. Reference-free single-pass EPI Nyquist ghost correction using annihilating filter-based low rank Hankel matrix (ALOHA). Magn Reson Med. 2016; 76(6):1775–1789. [PubMed: 26887895]
10. Lobos RA, Kim TH, Hoge WS, Haldar JP. Navigator-Free EPI Ghost Correction With Structured Low-Rank Matrix Models: New Theory and Methods. IEEE Trans Med Imaging. 2018; 37(11):2390–2402. [PubMed: 29993978]
11. Shin PJ, Larson PE, Ohliger MA, et al. Calibrationless parallel imaging reconstruction based on structured low-rank matrix completion. Magn Reson Med. 2014; 72(4):959–970. [PubMed: 24248734]
12. Cadzow JA. Signal enhancement-a composite property mapping algorithm. IEEE Transactions on Acoustics, Speech, and Signal Processing 1988; 36(1): 49–62 doi: 10.1109/29.1488.
13. Gavish M, Donoho DL. Optimal shrinkage of singular values. IEEE Trans Information Theory. 2017; 63:2137.
14. Van Huffel S Enhanced resolution based on minimum variance estimation and exponential data modeling. Singal Processing. 1993; 33:333–355.
15. Barash B, Gavish M. Optimal shrinkage of singular values under random data contamination. Neural Information Processing Systems (NIPS). 2017:6160–6170.
16. Tamir JI, Uecker M, Chen W, et al. T2 shuffling: Sharp, multicontrast, volumetric fast spin-echo imaging. Magn Reson Med. 2017; 77(1):180–195. [PubMed: 26786745]
17. Bilgic B, Kim TH, Liao C, Manhard MK, Wald LL, Haldar JP, Setsompop K. Improving parallel imaging by jointly reconstructing multi-contrast data. Magn Reson Med. 2018 8;80(2):619–32. [PubMed: 29322551]
18. Madore B, Glover GH, Pelc NJ. Unaliasing by fourier-encoding the overlaps using the temporal dimension (UNFOLD), applied to cardiac imaging and fMRI. Magn Reson Med. 1999; 42(5):813–828. [PubMed: 10542340]
19. Tsao J, Boesiger P, Pruessmann KP. k-t BLAST and k-t SENSE: dynamic MRI with high frame rate exploiting spatiotemporal correlations. Magn Reson Med. 2003; 50(5):1031–1042. [PubMed: 14587014]
20. Bydder M, Du J. Noise reduction in multiple-echo data sets using singular value decomposition. Magn Reson Imaging. 2006; 24(7):849–856. [PubMed: 16916702]
21. Jung Y, Samsonov AA, Bydder M, Block WF. Self-calibrated multiple-echo acquisition with radial trajectories using the conjugate gradient method. J Magn Reson Imaging. 2011 4;33(4):980–7. doi: 10.1002/jmri.22482. [PubMed: 21448967]

22. Pusterla O, Bauman G, Bieri O. Three-dimensional oxygen-enhanced MRI of the human lung at 1.5T with ultra-fast balanced steady-state free precession. Magn Reson Med. 2018; 79(1):246–255. [PubMed: 28337782]

23. Porter DA, Heidemann RM. High resolution diffusion weighted imaging using readout segmented echo planar imaging, parallel imaging and a two dimensional navigator based reacquisition. Magn Reson Med 2009;62(2):468–475. [PubMed: 19449372]

24. Hess AT, Robson MD. Hexagonal gradient scheme with RF spoiling improves spoiling performance for high-flip-angle fast gradient echo imaging. Magn Reson Med. 2017; 77(3):1231–1237. [PubMed: 27037941]

25. Kim TH, Haldar JP. LORAKS Software Version 2.0: Faster Implementation and Enhanced Capabilities. USC-SIPI Report #443, 2018.

26. Bydder M, Du J, Takahashi A, et al. Chemical shift artifact in center-out radial sampling: A potential pitfall in clinical diagnosis. Paper presented at: Proc Int Soc Magn Reson Med 2007.

27. Holland D, Kuperman JM, Dale AM. Efficient correction of inhomogeneous static magnetic field-induced distortion in Echo Planar Imaging. Neuroimage. 2010; 50(1):175–183. [PubMed: 19944768]

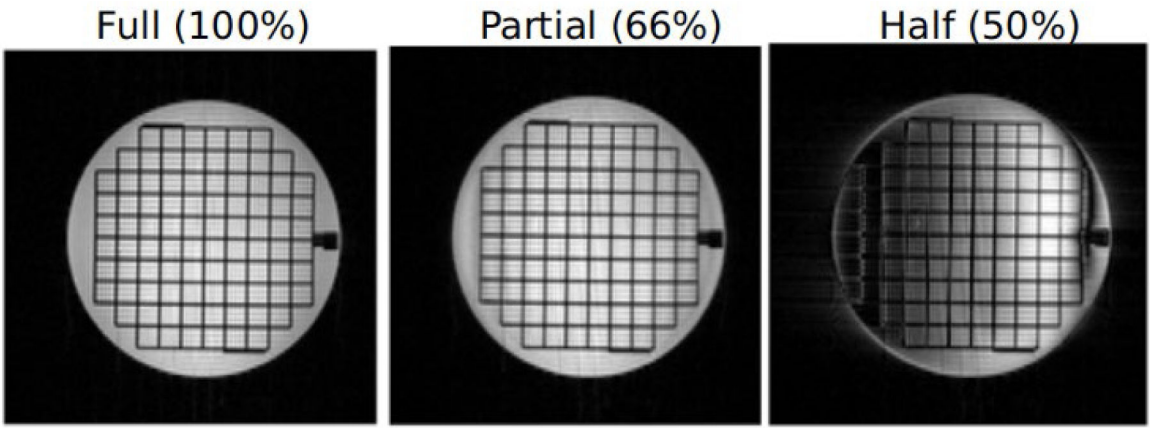

Figure 1:
Images from a SPGR dataset using different fractional echo factors (readout direction left-right) reconstructed by LORAKS. Scan parameters are as follows: SPGR, matrix 192, field of view 220 mm, bandwidth 200 Hz/pixel, TR 10 ms, TE 0.75–3.25 ms.

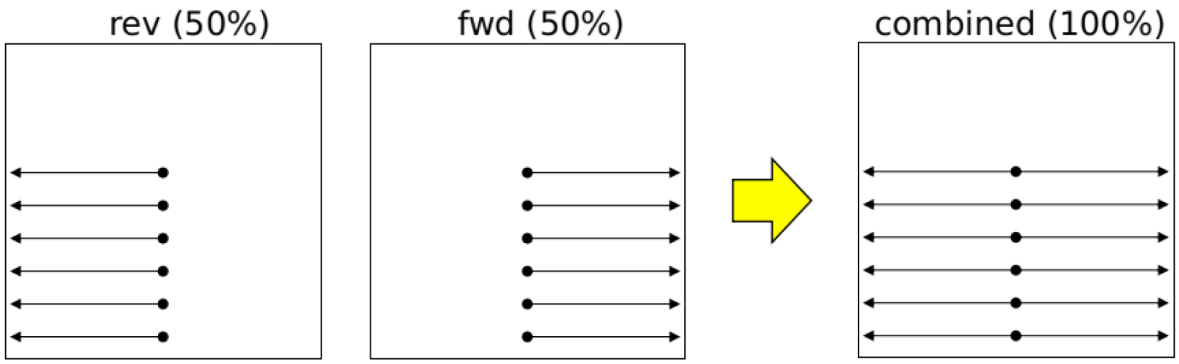

Figure 2:
Sampling scheme for a double half echo acquisition (left and middle) combined into a single *k*-space (right). Note the phase direction uses 5/8 partial Fourier to compensate for the doubling of acquisition time.

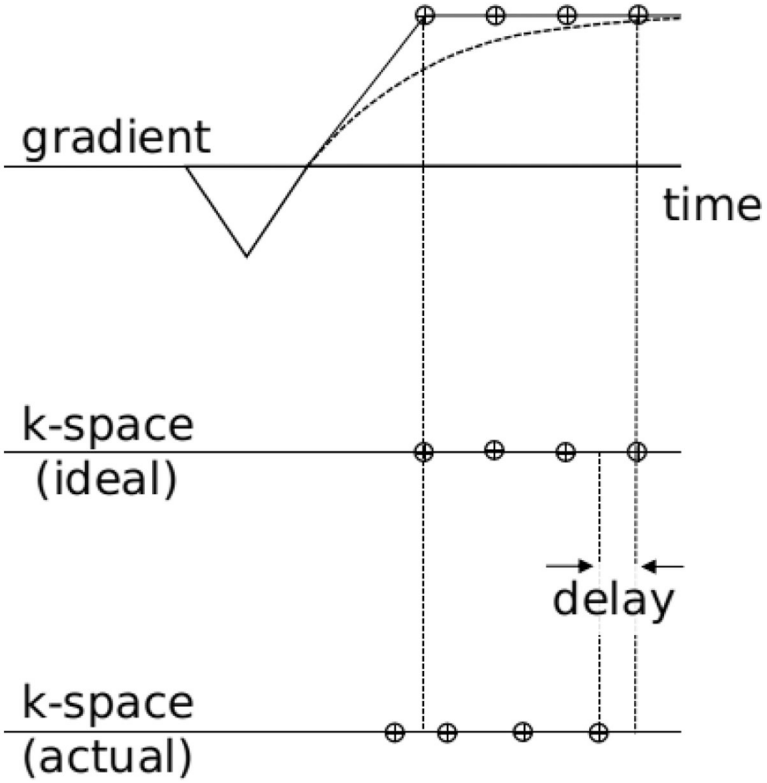

Figure 3:
Schematic of an ideal trapezoidal readout gradient (top row) subject to short term eddy currents that result in the actual gradient (dashed line). The sampled points map to different k-space co-ordinates (bottom rows).

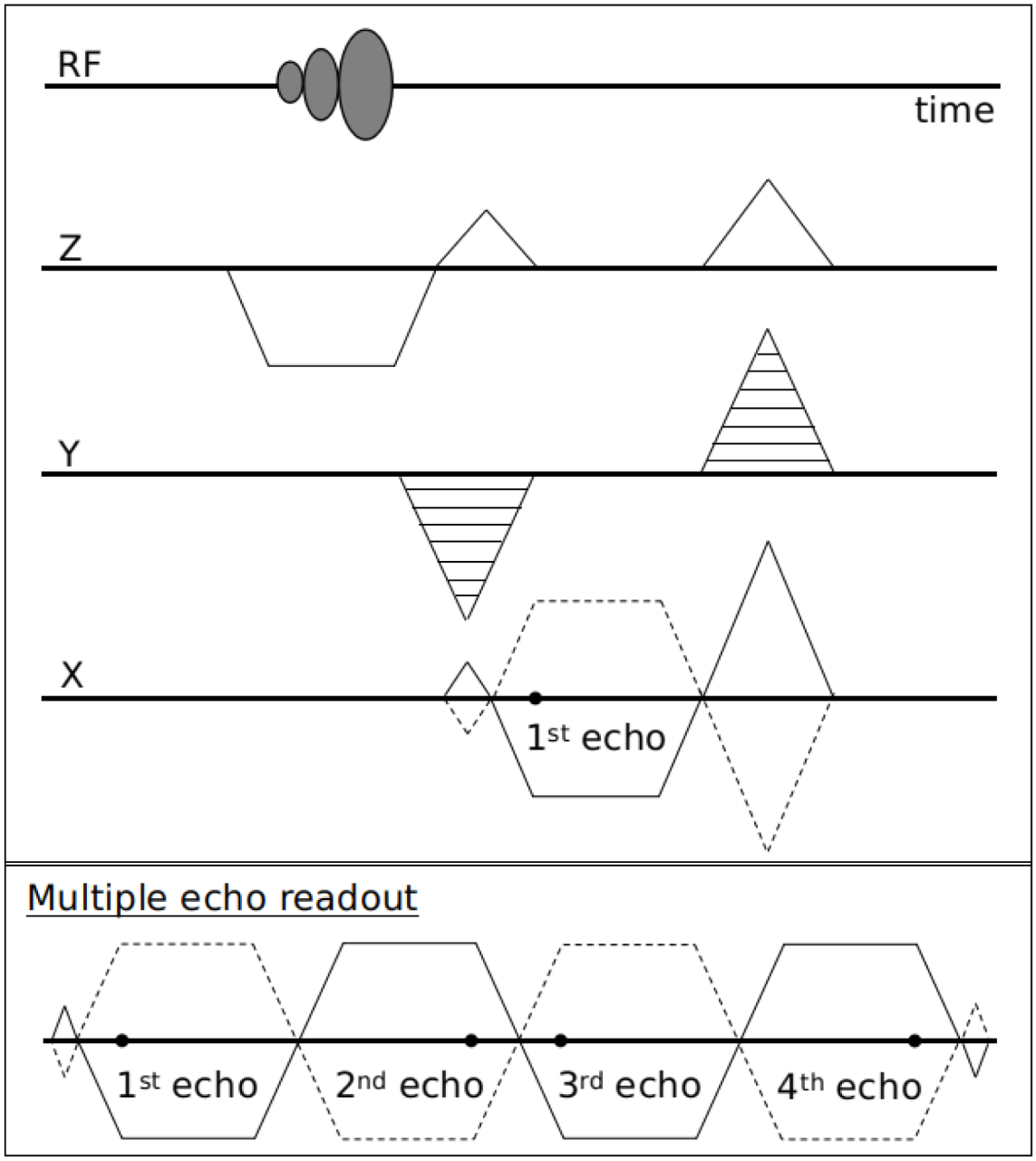

Figure 4:
Pulse sequence diagram for a bSSFP acquisition with the center of the echo indicated by a black dot. Forward and reverse readouts (from separate acquisitions) are represented by the solid and dashed lines. The bottom row shows an example of a multiple echo readout using half echoes; the echo spacing between the 2nd and 3rd echoes is very short but may be increased using a delay or higher echo fraction (e.g. 55% rather than 50%).

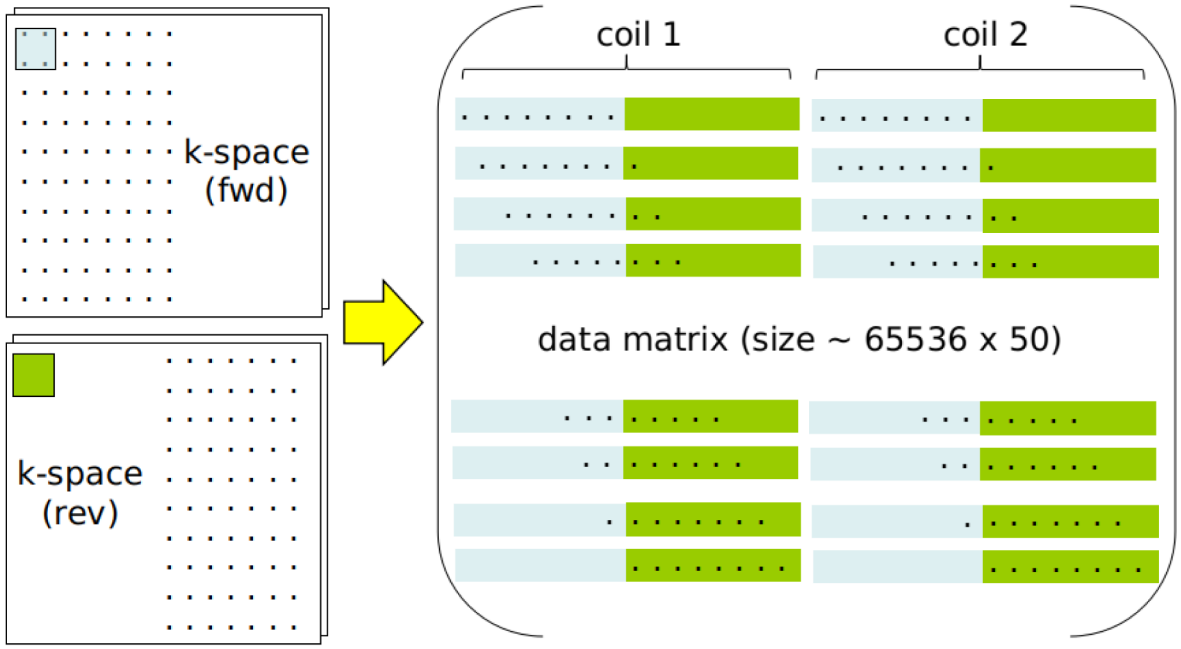

Figure 5:

Construction of the data matrix from forward (*fwd*) and reverse (*rev*) readouts and 2 coils. Each row of the data matrix consists of *k*-space points under the convolution kernel (small squares) for each coil while the kernel is moved through all of k-space. Missing samples are generated by a low rank matrix completion algorithm (Table 2).

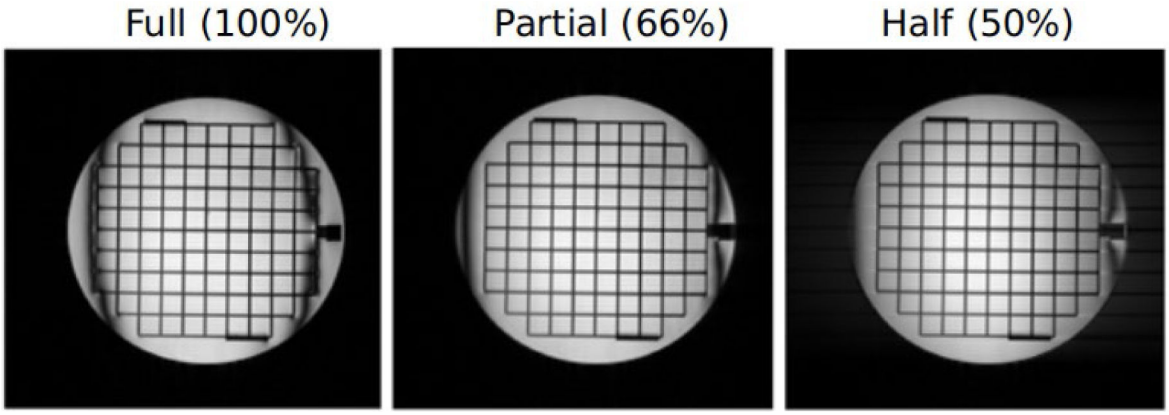

Figure 6:
Reconstructed bSSFP images using full sampling, partial sampling and half echoes. The decreasing TRs (given in Table 1) provide increased robustness to banding artefacts. Scan parameters: bSSFP, matrix 192, field of view 220 mm, bandwidth 200 Hz/pixel, TR and TE in Table 1.

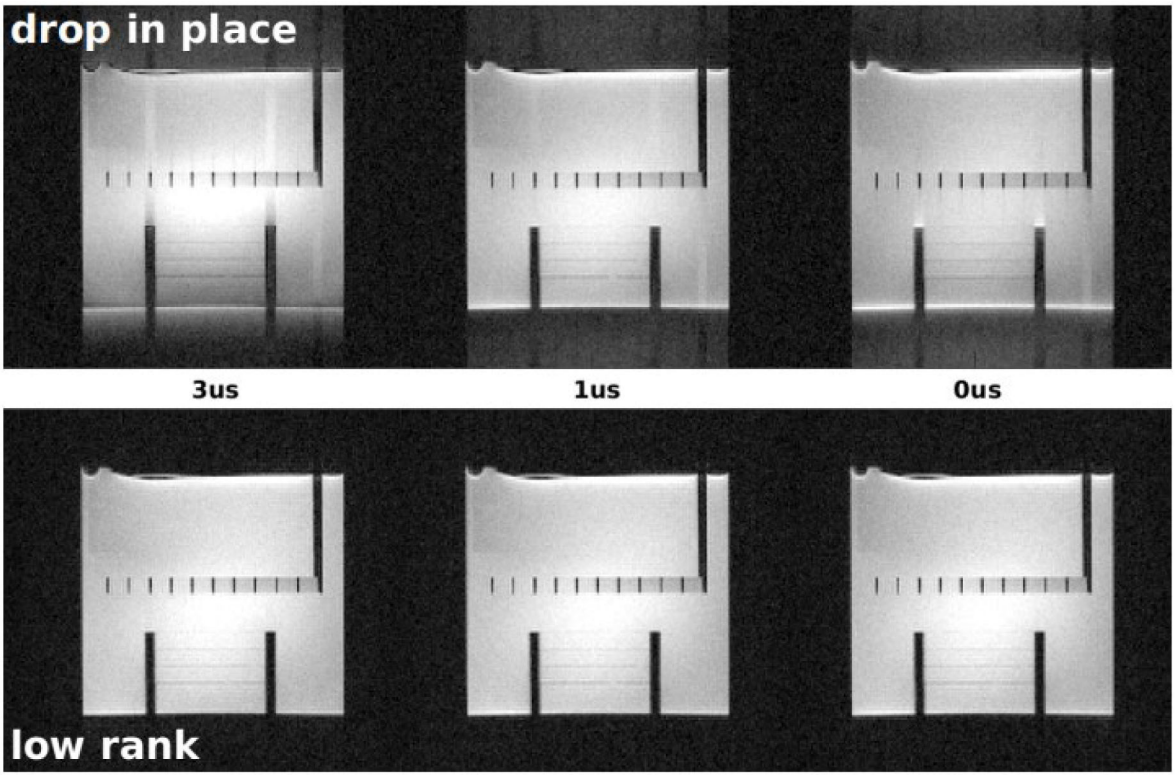

Figure 7:

Examples of datasets perturbed by delays of the readout gradient (up-down direction) using “drop in place” and low rank reconstructions. Window and level is adjusted to aid visualization of artefacts. The low rank method is robust to errors of several microseconds while the drop in place method is highly sensitive to delays. Scan parameters: bSSFP, matrix 256, field of view 220 mm, TR 2.5 ms, TE 1.2 ms, bandwidth 1395 Hz/pixel (dwell time 1.5μs).

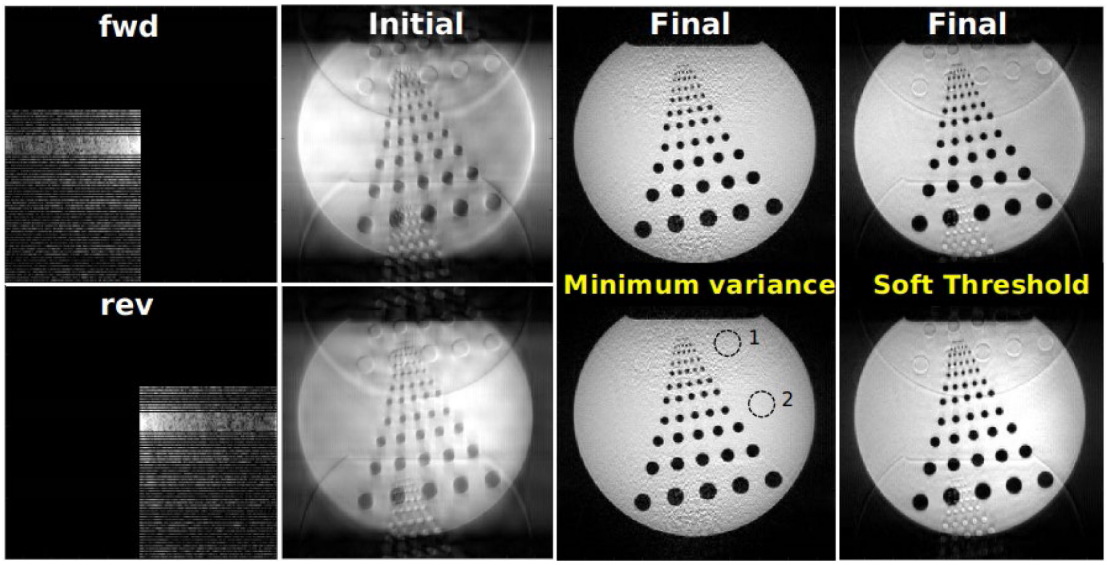

Figure 8:

Double half echo reconstruction with partial and parallel sampling in the phase encode direction. The left panels show the k-space sampling and images on the first iteration (before reconstruction). The right panels show images after 10000 iterations using two singular value filters. The minimum variance filter exhibits stronger g-factor noise enhancement and less aliasing compared to the soft threshold filter. Two ROIs correspond to the SNR results in Table 3. Scan parameters: SPGR, matrix 192, field of view 220 mm, bandwidth 200 Hz/pixel, TR 10 ms, TE 0.75 ms.

Table 1:

Examples of echo fraction, minimum echo time, echo spacing and repetition time are given for the following protocol: bSSFP, readout points 192, field of view 220 mm, bandwidth 200 Hz/px, RF pulse 0.6 ms.

Echo Fraction	Minimum TE (ms)	Minimum ΔTE (ms)	Minimum TR (ms)
100%	3.17	5.79	6.67
66%	1.53	4.96	5.03
50%	0.75	3.04	4.25

Table 2:

Outline of the iterative algorithm for finding *k*-space values that satisfy the conditions listed in the final column. Low rank constraints enforce consistency across the coil (parallel imaging), conjugate symmetry (partial Fourier) and half echo dimensions. The algorithm is similar to that proposed in Ref 11, which was based on Ref 12, and converges to a stable solution; however it is unclear what specific metric is optimized.

Initialize	**y = *k*-space data from fwd/rev readouts** **k = zero array the same size as y** **D = data sampling operator (binary)** **σ_{floor} = noise floor (see Appendix)**	**Condition**
1	Start of the iteration loop	
2	**k = k + D (y – k)**	Data consistency
3	Create data matrix **A** (see Figure 5)	Low rank constraints
4	[**U S V**] = svd(**A**,'econ')	
5	$f = \max(1 - \sigma^2_{floor} / \mathrm{diag}(\mathbf{S})^2, 0)$ $\mathbf{A} = \mathbf{A}\,\mathbf{V}\,\mathrm{diag}(f)\,\mathbf{V}^{\mathbf{H}}$	
7	**k** = average along anti-diagonals of **A**	Structural consistency
8	End of the iteration loop	

Table 3:

Comparison of the SNR (defined as mean/standard deviation) in two regions of interest (ROIs), indicated by circles in Figure 8, for fwd/rev datasets and the sum of squares combination. If the noise were independent then the SNR of latter would be 41% higher, however no difference is seen reflecting the highly correlated noise.

Dataset	SNR: ROI 1	SNR: ROI 2
fwd	9.15	20.88
rev	9.16	24.47
combined	9.15	22.62